Electrochimica Acta 334 (2020) 135541

Contents lists available at ScienceDirect

Electrochimica Acta

journal homepage: www.elsevier.com/locate/electacta

Non-constancy of the bulk resistance of ionophore-based Cd^{2+}-selective electrode: A correlation with the water uptake by the electrode membrane

Andrey V. Kalinichev, Elena V. Solovyeva, Arina R. Ivanova, Galina A. Khripoun, Konstantin N. Mikhelson*

Chemistry Institute c/o St.Petersburg State University, 26 Universitetsky Prospect, Stary Peterhof, 198504, St.Petersburg, Russia

ARTICLE INFO

Article history:
Received 13 August 2019
Received in revised form
4 October 2019
Accepted 16 December 2019
Available online 18 December 2019

Keywords:
Ionophore-based ion-selective membranes
Cadmium
Bulk resistance
Water uptake
Correlation

ABSTRACT

The dependence of the bulk resistance of Ion-selective electrodes (ISEs) on the concentration of aqueous solution is studied by means of chronopotentiometry and electrochemical impedance using Cd^{2+}-ISE as model system. It is shown that within the Nernstian response range that bulk resistance of the ISE membrane increases along the dilution of the aqueous phase. The results are consistent with analogous studies carried out earlier with Ca^{2+}, K^+ and NO_3^--ISEs. Water uptake by the Cd^{2+}-ISE membrane is studied systematically, and it is shown that the water uptake also increases along decrease of the concentration of $CdCl_2$ solution. The shapes of the concentration dependence of the two properties: (1) the membrane bulk resistance and (2) the water uptake, are very similar, suggesting a correlation between (1) and (2). SEM/EDX studies of Cd^{2+}-ISE membranes confirm uniform distribution of the components within dry membranes, except of surface layers which are enriched in plasticizer and depleted in the polymer. It is concluded that the ISE membranes equilibrated with aqueous solutions must be considered as non-homogeneous materials due to the presence of the dispersed water. It is assumed that the electrochemical equilibrium is established between the solution and the membrane organic phase proper, while the resistance refers to the membrane as a material including water droplets which hinder the charge transfer across the membranes.

1. Introduction

Ionophore-based ion-selective electrodes (ISEs) are routinely used in a large number of applications as sensors with various signal transduction modes: potentiometric [1–5], voltammetric [6–12], and ampero- and coulometric mode [13–18]. Currently, potentiometry remains the most frequently used mode of the measurements with ISEs. The theory of the potentiometric response and selectivity of ISEs is very well developed, describing not only the boundary potential at the membrane/solution interface, but also the diffusion potential within the membrane and the potential generation over real time and space [2,4,19–24].

In spite of this, experimental evidences exist which are in conflict with the theory. We mean here the dependence of the bulk resistance of ISE membranes on the concentration of the aqueous phase [25–27]. This dependence is in conflict with the theory because of the following. The overall membrane potential can be considered as a superposition of three components [4,19,20]. Two of these are boundary potentials: one at the membrane/sample interface, and the other one at the interface between the membrane and the internal reference system: an internal solution or a solid contact, e.g. a conducting polymer. The third component is the diffusion potential within the membrane. Simple theories consider only the boundary potential [28], those more advanced consider also the diffusion potential [20–24]. Whatever the level of the theory, all of these predict, for the Nernstian response range, a constant value of the activity of the target ion within the whole membrane. According to theory, a non-constant value of the target ion activity at the outer surface of the membrane results in deviations from the Nernstian response. Further deviations originate from the non-zero diffusional potential which generates in the case of a non-flat profile of the target ion activity across the membrane.

* Corresponding author.
E-mail addresses: konst@km3241.spb.edu, k.mikhelson@spbu.ru (K.N. Mikhelson).

https://doi.org/10.1016/j.electacta.2019.135541
0013-4686/

Thus, within the Nernstian response range the target ion activity must be constant in the whole membrane, and therefore one should also expect a constant composition of the membrane phase within this region. In turn, this implies a constant value of the membrane bulk resistance over the Nernstian response range. So, according to theory, a single sensor cannot show both a potentiometric and a conductometric response. However, some time ago we reported on such sensor [29]. Recently, we re-visited this issue, and demonstrated the non-constancy of the bulk resistance of ISEs selective to Ca^{2+} [25], to NO_3^- [26] and to K^+ [27], within the Nernstian response range: the resistance increases along decrease of the concentration of the respective electrolyte. Importantly, the non-constancy of the bulk resistance is more pronounced at the electrolyte concentrations below 10^{-3} M, while at higher concentrations the value of the bulk resistance is less dependent on the concentration of the solution. This means that the effect cannot be due to co-extraction of aqueous electrolyte, because in such a case the dependence intensifies at higher concentrations [2,19,20]. Tentatively, we ascribed this dependence to water uptake by the ISE membranes. For decades, it is known that membranes consisting of plasticized poly (vinyl chloride) and containing ionophores sorb water from aqueous solutions, and become turbid due to the Rayleigh scattering of light on water droplets [30–34]. It was suggested that the droplets act as traps for anions (OH^-), and in this way ensure cationic response of ISEs containing only neutral ionophores, and no ion-exchanger sites in membranes [30]. Harrison's group performed a systematic study of water uptake, and showed that water in membranes forms droplets with sizes ca. 15–20 nm [31–34]. They reported on a water-enriched surface region in membranes [32], and on the existence of two kinds of absorbed water characterized by diffusion coefficients D of $1.5 \cdot 10^{-6}$ and $4.3 \cdot 10^{-7}$ cm^2/s [34]. It was suggested that the use of $CoCl_2$ for optical tracing of water by the Harrison's group biased the results, and in fact water droplets exist only in the surface layer of the membrane (within 100 μm from the interface) [35]. More recently the existence of monomeric, dimeric, clustered and bulk water in membranes was registered by FTIR-ATR [36] and by hyphenated FTIR-ATP and impedance studies [37,38]. Furthermore, the existence of two kinds of absorbed water: a "faster" – monomeric and dimeric water, and "slower" – clustered and bulk water has been reported for acrylic and silicon rubber membranes [39]. Thus, water uptake and formation of water droplets in membranes is a well-established fact, however where is only a little data on the dependence of water uptake on the concentration of the solution [34,40].

Our preliminary studies showed remarkable water uptake by Cd^{2+}-membranes containing commercially available Cadmium Ionophore I in poly (vinylchloride) plasticized with 2-nitrophenyloctyl ether. This is why we have chosen Cd^{2+}-ISEs based on this well-known ionophore for a systematic study of the membrane bulk resistance together with water uptake, using the same protocols as before [25–27] for better compatibility of the results. This allowed obtaining, for the first time, reliable data on the dependence of water uptake on the concentration of the electrolyte in solution, over a wide range. Furthermore, we show here for the first time that the membrane bulk resistance correlates with water uptake.

2. Experimental

Cadmium ionophore I *N*,*N*,*N*′,*N*′-tetrabutyl-3,6-dioxaoctanedi (thioamide), (ETH 1062), potassium tetrakis-(4-chlorophenyl) borate (KClTPB), lipophilic salt tetradodecylammonium tetrakis-(4-chlorophenyl)borate (ETH 500), solvent plasticizer 2-nitrophenyloctylether (oNPOE), high molecular weight poly (vinyl chloride) (PVC) were Selectophore grade reagents from Fluka (Switzerland). Volatile solvents were extra pure cyclohexanone (CH) and HPLC grade tetrahydrofuran (THF) from Vekton (St. Petersburg, Russia). Inorganic salts were from Reaktiv (Moscow, Russia). All aqueous solutions were prepared with deionized (DI) water with resistivity 18.2 MOhm · cm (Milli-Q Reference, Millipore, France).

The membrane cocktails were prepared by dissolving appropriate amounts of PVC and oNPOE in THF. After that, ETH 1062, KClTPB and ETH 500 were added as appropriate aliquots of stock solutions in cyclohexanone. This allowed avoiding taking small weights and ensured high accuracy of the membrane composition. To obtain the membranes, the cocktails were stirred for 30 min using roller-mixer Selecta Movil Rod (Spain) and then cast on glass Petri dishes with diameter of 50 mm. The dishes were closed with filter paper to slow down the evaporation of volatile solvents. The complete evaporation of THF and CH took 2 days, and after that master membranes with a thickness of about 0.7 mm were obtained. Two membranes (M1 and M2) were prepared, each contained 460 mg PVC, 920 ml oNPOE, 8.0 mg ETH 1062 and 4.5 mg KClTPB. The molar excess of ionophore over sites was 2 : 1. Membrane M2 also contained 10.5 mg ETH 500 (in 1:1 M ratio to KClTPB).

The electrodes were prepared by cutting disks with diameter of 12 mm from the master membrane and gluing them to PVC bodies with the outer diameter of 12 mm and the inner diameter of 10 mm. A solution of PVC in CH was used as the glue. The internal reference electrode was chlorinated silver wire in a polypropylene body. The electrode construct is shown in Fig. S1 (Supplementary Data).

Initially, the ISEs were filled with 0.01 M $CdCl_2$ and conditioned in this solution. In our previous studies 3 days were enough to obtain stable values of the membrane resistance although to be sure about the results the soaking time was actually longer, up to 1 week [25–27]. In the case of Cd^{2+}-ISEs, according to preliminary studies, the membrane resistances became stable only after a week of soaking. Apparently, the replacement of K^+ ions (from KClTPB) by Cd^{2+} in the whole membrane bulk is relatively slow. Therefore, to be on the safe side, we let the ISEs soak for 2 weeks.

After that, zero-current EMF measurements, chronopotentiometric measurements, and impedance measurements have been performed in $CdCl_2$ solutions. Zero current potentiometric measurements were performed with Ecotest-120 8-channel potentiometric station (Econics, Russia). The reference electrode was a single junction Ag/AgCl electrode in 3.5 M KCl, with a salt bridge with a limited leak of KCl. Calibration in $CdCl_2$ solutions was performed from 0.1 M down to 10^{-8} M $CdCl_2$ using automatic burette Metrohm 700 Dosino controlled by Metrohm 711 Liquino Controller.

Chronopotentiometric curves and electrochemical impedance spectra were recorded with Potentiostat-Galvanostat Autolab 302 N with a frequency response analyzer module FRA 2 (Metrohm, Switzerland). The ISE membranes always have two surfaces: one in contact with the sample or calibration solution, and the other one in contact with the internal reference system (the internal solution or a solid contact). Both respective interfaces contribute to the measured signals. Therefore, if the property of interest refers exactly to the membrane, the respective electrochemical cell must be symmetric: the internal and the external solutions, as well as the reference electrodes must be the same. We used chlorinated silver wires as the reference electrodes, and glassy carbon rod as counter electrode, like in our earlier studies [25–27,41,42].

The protocol of the chronopotentiometric measurements was the same as used before [25–27]. The open circuit potentials (OCPs) were recorded for the first 10 s, then the current value was abruptly

changed from zero to 10^{-7} A (the respective current density was $2.88 \cdot 10^{-7}$ A/cm^2) and the potential was registered for 60 s. After that the current was turned off, and the potential was registered for another 60 s. The time resolution in chronopotentiometry measurements was always 0.2 s.

The impedance measurements were made in potentiostatic mode with the excitation magnitude of ±5 mV around the OCP, within the frequency range from 100 kHz to 0.01 Hz.

All electrochemical measurements were carried out in a plastic beaker with a volume of 50 ml, at room temperature (22 ± 1 °C). Five replicate electrodes with each membrane composition (ISEs 1–5 with membrane M1 and ISEs 6–10 with M2) were used in this work.

Activities of Cd^{2+} ion in solutions were calculated according to the Davis' equation (3rd approximation of the Dubye-Hűckel theory):

$$\log\gamma_I = -\frac{0.512 z_I^2 \sqrt{J}}{1 + a_{Kjel} \cdot 0.328\sqrt{J}} + 0.1 z_I J \quad (1)$$

Here γ_I is the ion activity coefficient, z_I is the ion charge number, J is the solution ionic strength, and a_{Kiel} is the Kielland parameter (5 for Cd^{2+}) [43].

SEM/EDX studies were performed with Carl Zeiss Merlin electron microscope with field emitting cathode and electron optical column Gemini-II in the *Interdisciplinary Center for Nanotechnology*, Research Park of St. Petersburg State University.

3. Results and discussion

3.1. EMF measurements

The potentiometric performance of Cd^{2+}-ISEs based on ETH 1062 as ionophore already has been studied elsewhere [44]. This study was focused on the bulk resistance of the membranes of Cd^{2+}-ISEs within the Nernstian response range. Therefore, our potentiometric studies were limited to check the linear range of the ISEs response in $CdCl_2$ solutions, and the selectivity to Cd^{2+} over Na^+. The latter ion was chosen because of its abundance.

The response curves obtained by sequential 10-fold dilution of 0.1 M $CdCl_2$ with DI water down to 10^{-8} M are shown in Figs. S2 and S3. In each solution, the EMF was recorded for 300 s, and the average signal for the last 100 s was used to plot the calibration curves shown in Figs. 1 and 2.

The ISEs showed linear response to Cd^{2+} from 0.1 to 10^{-5} M $CdCl_2$ with the slopes 26.2 ± 0.1 (ISEs 1–5) and 24.6 ± 0.2 (ISEs 6–10) mV/log (a_{Cd}), and lower detection limits log (a_{Cd}) −5.60 and −5.54, respectively. The EMF values recorded in 0.1 M $CdCl_2$ and in 0.1 M NaCl were used to measure the selectivity to Cd^{2+} over Na^+ ions, and the selectivity coefficient was calculated by the equation known for the case of a divalent primary ion and a monovalent interfering ion [19,45]:

$$E = E^0 + \frac{RT}{F}\ln\left(\sqrt{a_{Ca} + \frac{1}{4}Ka_{Na}^2} + \sqrt{\frac{1}{4}Ka_{Na}^2}\right) \quad (2)$$

The results were $\log K_{Cd/Na} \approx -2.5 \pm 0.2$ for both kinds of the ISEs: 1–5 and 6–10. These data confirmed the suitability of the ISEs for further studies.

3.2. Chronopotentiometric studies

The resistance and capacitance values of the ISEs were measured by chronopotentiometric and impedance techniques. Concentration of $CdCl_2$ varied from 10^{-5} to 10^{-1} M, i.e. within the linear Nernstian response range of the ISEs. Polarization of the Ag/AgCl electrodes in contact with 10^{-3} M and more concentrated $CdCl_2$ solutions, as well as the impact from the solution resistance were negligible as compared with the polarization of the membranes. However, in the case of 10^{-5} and 10^{-4} M $CdCl_2$, chronopotentiometric curves obtained with ISEs were corrected for the polarization of Ag/AgCl electrodes and for the solution resistance. For this purpose additional measurements were performed without PVC membranes.

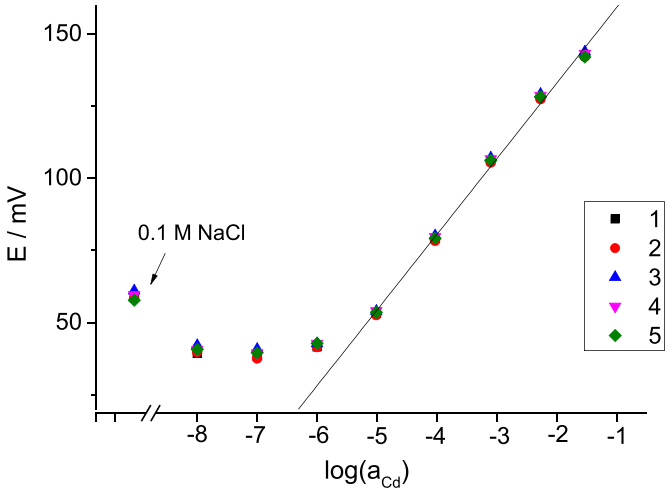

Fig. 1. EMF values obtained with ISEs 1–5 (membrane M1 without ETH 500) in $CdCl_2$, and in 0.1 M NaCl. Numbers in the legend refer to the individual ISE numbers. Straight line refers to ISE 1.

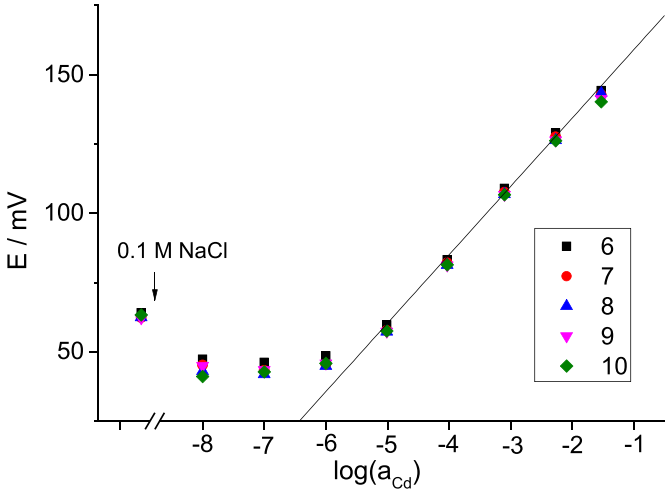

Fig. 2. EMF values obtained with ISEs 6–10 (membrane M2 with ETH 500) in $CdCl_2$, and in 0.1 M NaCl. Numbers in the legend refer to the individual ISE numbers. Straight line refers to ISE 6.

Chronopotentiometric curves obtained with ISEs 1 (membrane M1 without ETH 500) and 6 (membrane M2 with ETH 500) corrected for the solution resistance and for the polarization of Ag/AgCl electrode are shown in Fig. 3.

In the initial parts of the curves: before the polarizing current was turned on, the recorded potentials were close to zero due to the symmetry of the cell. At time t = 10 s the current was turned on resulting in a positive Ohmic potential drop followed with a polarization curve. At time t = 70 s the current was turned off causing a negative Ohmic drop followed with a relaxation curve. The main

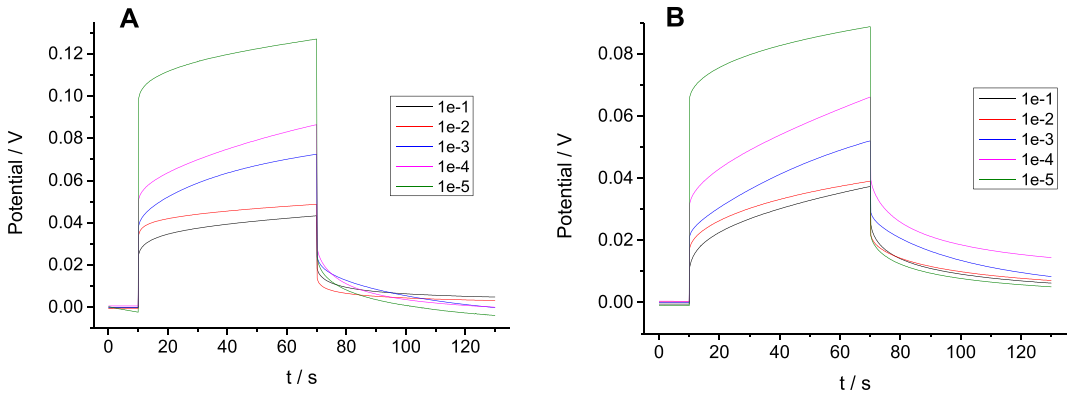

Fig. 3. Chronopotentiometric curves obtained in $CdCl_2$ solutions with ISEs 1 (A) and 6 (B).

impact to the Ohmic drops obtained in chronopotentiometric measurements is due to the bulk resistance of the ISEs. However, the impedance measurements (see below) showed that chronopotentiometry slightly overestimates the bulk resistance of the ISEs under study. Similar effect was obtained for NO_3^--ISEs [26]. The main trend, however, is clear: the Ohmic drop values (and, respectively, also the membrane bulk resistances) increases along the dilution of $CdCl_2$. In our earlier studies with Ca^{2+}-ISEs [25] and K^+-ISEs [27], the chronopotentiometric curves were almost Π-shaped: the Ohmic drops values were much larger than the impacts from polarization and relaxation. In this case, like observed earlier with NO_3^--ISEs [26], the polarization and relaxation values are comparable with the Ohmic drops. At least partly, this is because of lower resistance of Cd^{2+} membranes due to the use of oNPOE as plasticizer. Typically, the magnitudes of the positive and the negative Ohmic drops (and the values of the membrane bulk resistance calculated from the drops magnitudes) were the same within ±2%, although sometimes this discrepancy increased to ± 7%. There was no regularity about the increase of the non-equality of the positive and negative Ohmic drops. The mean values of the membrane bulk resistance obtained from the Ohmic drops in chronopotentiometric measurements, and the respective standard deviations are collected in Table 1, the whole set of the data is given in Table S1 (Supplementary Data).

We have shown earlier [25–27] that the polarization and relaxation curves can be fitted to an equation which combines an exponential decay and a term which originates from the concentration polarization:

$$\eta = iR_{expon}(1 - \exp(-t/\tau)) + iN\sqrt{t} \quad (3)$$

Here η is the polarization (or relaxation), i is the polarizing current density, R_{expon} is the resistance which refers to the decaying exponent with τ the characteristic time, t is time from the moment when current was turned on or off, N is a coefficient related to the transportation impact to polarization or relaxation. Experimental curves were fitted to Eq. (3) with *OriginLab* Origin 9 software. Examples of the experimental and fitted curves are shown in Figs. S4 and S5. The values of R_{expon} obtained from polarization and from relaxation curves scattered from 16 to 90 kΩ for ISEs with and without ETH 500, and did not show any regular dependence on the $CdCl_2$ concentration in solution. Values of the respective capacitances calculated as $C_{expon} = \tau/R_{expon}$ scattered around 50 μF and sometimes were up to 100 μF. The lack of regular dependence of R_{expon} on the $CdCl_2$ concentration, together with very large C_{expon}, mean that these values cannot be ascribed to the charge transfer resistance and the double layer capacitance at the membrane/solution interface. Analogous results we obtained earlier with calcium and potassium ISEs [25,27]. Increase of the overall polarization along the dilution of the aqueous phase seen in Fig. 3 A, B is due to increased concentration polarization.

The kinetics of the change of the ISE bulk resistance in response to the change of the solution concentration was studied in a way analogous to our studies with Ca^{2+}, NO_3^- and K^+ electrodes [25–27]. Initially, ISEs were stored in 10^{-2} M $CdCl_2$ (and filled with the same solution) for 24 h, and then chronopotentiometric curves were recorded. After that the solutions: external and internal, were replaced with 10^{-4} M $CdCl_2$. The manipulations needed for the solution replacement took about 1 min. Chronopotentiometric curves in 10^{-4} M $CdCl_2$ were recorded at 3 min after the replacement, and then several times over a period of 15 h. After that, the procedure was reversed: 10^{-4} M $CdCl_2$ was replaced with 10^{-2} M $CdCl_2$, and the measurements were done in the same way. The results are presented in Fig. 4. Like earlier in the case of calcium and

Table 1
The mean values of the membrane bulk resistance obtained from the Ohmic drops in chronopotentiometric measurements.

Concentration of $CdCl_2$, M	R_{bulk} (from the positive Ohmic drop), MΩ	SD, MΩ	R_{bulk} (from the negative Ohmic drop), MΩ	SD, MΩ
ISEs 1–5 (membrane M1 without ETH 500)				
$1\cdot10^{-1}$	0.33	0.04	0.33	0.04
$1\cdot10^{-2}$	0.40	0.07	0.41	0.07
$1\cdot10^{-3}$	0.52	0.07	0.49	0.06
$1\cdot10^{-4}$	0.56	0.06	0.56	0.06
$1\cdot10^{-5}$	1.1	0.3	1.1	0.4
ISEs 6–10 (membrane M2 with ETH 500)				
$1\cdot10^{-1}$	0.17	0.03	0.18	0.04
$1\cdot10^{-2}$	0.17	0.05	0.19	0.06
$1\cdot10^{-3}$	0.25	0.04	0.24	0.04
$1\cdot10^{-4}$	0.35	0.04	0.36	0.05
$1\cdot10^{-5}$	1.28	0.09	1.28	0.09

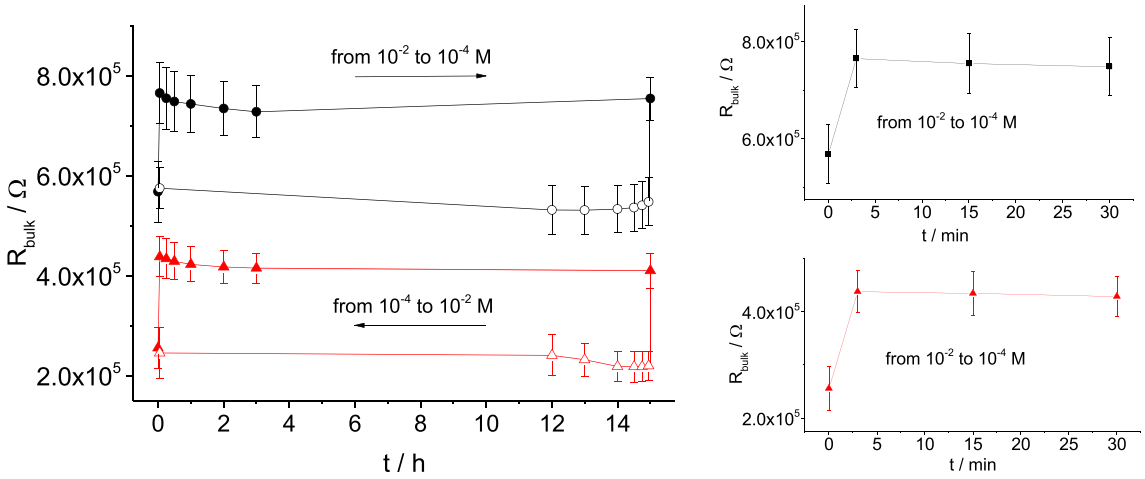

Fig. 4. The kinetics of the ISE membrane bulk resistance when the concentration of the aqueous solution is changed. Solid symbols refer to the replacement of 10^{-2} M $CdCl_2$ with 10^{-4} M, and open symbols to the reversed procedure, circles to ISEs 1–5 and triangles to ISEs 6–10. Insets show the change of the membranes bulk resistance during the first 30 min after the replacement of 10^{-2} M with 10^{-4} M $CdCl_2$.

potassium ISEs [25,27], most of the change of the resistance happened within 3 min after the replacement of the solutions, and only minor changes happened during the next 15 h.

3.3. Electrochemical impedance studies

The impedance spectra of the ISEs were measured with the electrodes equilibrated with $CdCl_2$ solutions with concentrations from 10^{-5} to 0.1 M. The examples of the spectra (Nyquist plots) are shown in Fig. 5.

The shape of the spectra recorded in 10^{-5} M $CdCl_2$ suggests negative values of Z_{real} at highest frequencies. Apparently, this is an artefact caused by polarization of Ag/AgCl electrodes at low concentrations of Cl^- anions.

The spectra were fitted to a circuit containing three sub-circuits in series (see Fig. 6). Each of the sub-circuits contained a resistor and a constant phase element in parallel, respectively R_1Q_1, R_2Q_2 and WQ_3, with W for Warburg resistance. An example of the fitting is shown in Fig. 6.

The R_1 values varied from 0.4 to 1.5 MΩ, increasing along decrease of the solution concentration, see Fig. 5. The Q_1 values were $(4 \pm 2) \cdot 10^{-10}$ $F \cdot s^{n-1}$ with the n factor from 0.90 to 0.96 (i.e. close to 1), and without regular dependence on the concentration of $CdCl_2$ solutions, or on presence or absence of ETH 500 in the membrane. These values suggest that R_1 and Q_1 are the bulk resistance and geometric capacitance of the membrane. The R_2 values varied from 40 to 400 kΩ without any regularity. The Q_2 values were $(3 \pm 2) \cdot 10^{-7}$ $F \cdot s^{n-1}$ with the n factor 0.7–0.9. Thus, Q_2 is far from an ideal capacitor. The mean values of the resistors and constant phase elements obtained from the impedance spectra of the ISEs equilibrated with $CdCl_2$ solutions with different concentrations are collected in Table 2.

Importantly, the time constant $\tau = R_2 \cdot Q_2$ value was in between 0.8 and 120 ms, well below the time resolution in the chronopotentiometric experiments (0.2 s). This is why this part of the circuit was not seen in chronopotentiometry. Respectively, the bulk resistances obtained from the Ohmic drop values were overestimated by the values of R_2. However, both techniques: chronopotentiometry and impedance show the same trend: increase of the bulk resistance along the dilution of the aqueous phase, as shown in Fig. 7. Thus, the data obtained with Cd^{2+}-ISEs are fully consistent with those obtained with calcium, nitrate and potassium ISEs [25–27].

Interestingly, addition of constant phase element Q_3 in parallel to Warburg resistance allowed for fitting straight lines with slopes different from 1. Values of Q_3 were $2 \cdot 10^{-7}$ – $3 \cdot 10^{-6}$ $F \cdot s^{n-1}$ with factor n about 0.2–0.5.

Recording impedance spectra takes time, therefore we did not study the kinetics of the change of the resistance by this method.

3.4. Measurements of water uptake by the membranes

In our previous studies we, tentatively, ascribed the non-constancy of the membrane bulk resistance to water uptake by the membranes [25–27]. One should expect a constant value of the water uptake when the membranes are in contact with diluted

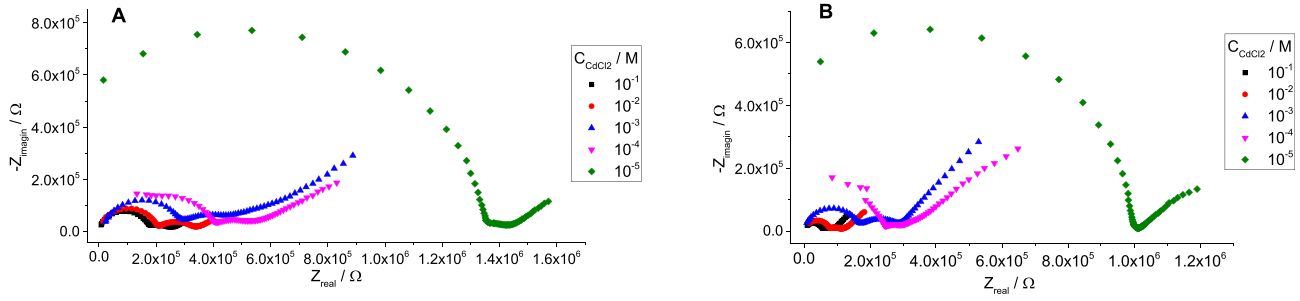

Fig. 5. Impedance spectra of ISE 1 (A) and ISE 6 (B). Concentrations of $CdCl_2$ solutions are shown in the legends.

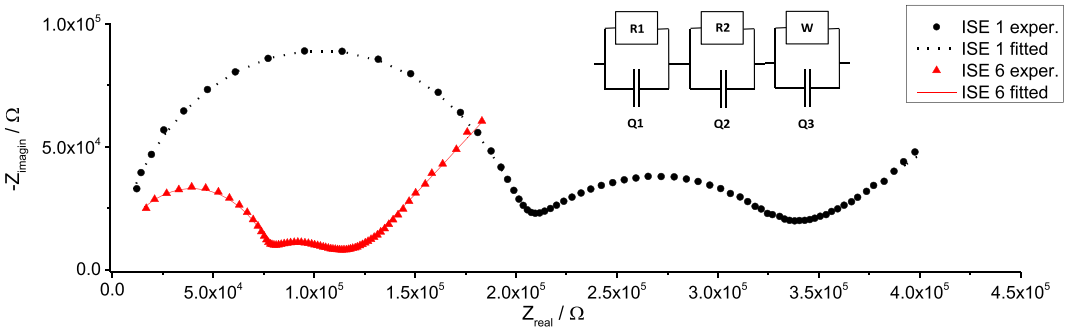

Fig. 6. Fitting of the impedance spectra of ISE 1 (without ETH 500) and ISE 6 (with ETH 500) recorded in 0.01 M $CdCl_2$. Inset shows the circuit used for the fitting of the spectra.

Table 2
Mean values of the high-frequency and low-frequency resistors and constant phase elements obtained from the impedance spectra.

Concentration of $CdCl_2$, M	R_1, MΩ	Q_1, $F \cdot s^{n-1}$	n_1	R_2, MΩ	Q_2, $F \cdot s^{n-1}$	n_2
ISEs 1–5 (membrane M1 without ETH 500)						
$1 \cdot 10^{-1}$	0.19 ± 0.03	$(3.3 \pm 0.3) \cdot 10^{-10}$	0.93 ± 0.02	0.12 ± 0.04	$(3.3 \pm 0.9) \cdot 10^{-7}$	0.75 ± 0.04
$1 \cdot 10^{-2}$	0.22 ± 0.02	$(1.7 \pm 0.2) \cdot 10^{-10}$	0.90 ± 0.06	0.18 ± 0.06	$(2.2 \pm 0.8) \cdot 10^{-7}$	0.81 ± 0.05
$1 \cdot 10^{-3}$	0.28 ± 0.05	$(1.6 \pm 0.2) \cdot 10^{-10}$	0.93 ± 0.02	0.31 ± 0.09	$(2 \pm 1) \cdot 10^{-7}$	0.82 ± 0.06
$1 \cdot 10^{-4}$	0.41 ± 0.03	$(4 \pm 1) \cdot 10^{-10}$	0.91 ± 0.03	0.09 ± 0.02	$(2.5 \pm 0.5) \cdot 10^{-7}$	0.73 ± 0.03
$1 \cdot 10^{-5}$	1.0 ± 0.2	$(3 \pm 1) \cdot 10^{-10}$	0.93 ± 0.03	0.11 ± 0.02	$(4.3 \pm 0.9) \cdot 10^{-7}$	0.77 ± 0.06
ISEs 6–10 (membrane M2 with ETH 500)						
$1 \cdot 10^{-1}$	0.059 ± 0.009	$(2.0 \pm 0.3) \cdot 10^{-10}$	0.91 ± 0.04	0.06 ± 0.02	$(2.6 \pm 0.5) \cdot 10^{-7}$	0.81 ± 0.03
$1 \cdot 10^{-2}$	0.089 ± 0.009	$(2.4 \pm 0.5) \cdot 10^{-10}$	0.92 ± 0.02	0.12 ± 0.06	$(4.7 \pm 0.6) \cdot 10^{-7}$	0.80 ± 0.04
$1 \cdot 10^{-3}$	0.11 ± 0.02	$(6 \pm 1) \cdot 10^{-10}$	0.93 ± 0.02	0.03 ± 0.02	$(4 \pm 1) \cdot 10^{-7}$	0.89 ± 0.04
$1 \cdot 10^{-4}$	0.25 ± 0.03	$(2.0 \pm 0.6) \cdot 10^{-10}$	0.96 ± 0.02	0.9 ± 0.2	$(3.0 \pm 0.7) \cdot 10^{-7}$	0.77 ± 0.05
$1 \cdot 10^{-5}$	1.0 ± 0.1	$(3.8 \pm 0.9) \cdot 10^{-10}$	0.93 ± 0.03	0.17 ± 0.06	$(4 \pm 1) \cdot 10^{-7}$	0.78 ± 0.04

solutions because the chemical potential of water in pure water and in electrolyte solutions with concentrations up to ca 1 M is almost the same. However, consideration of the interplay between the osmotic pressure of the external solution, that of water droplets, and the elastic pressure associated with the formation of pockets in the membrane (to accommodate droplets) allowed concluding that water uptake must increase along decrease of the ionic strength of the solution [34]. This conclusion got indirect experimental support [34]. More recently it was shown by Karl Fisher titration and by FTIR-ATR methods that water uptake from deionized water is several times larger than that from 0.1 $CaCl_2$, and the authors assign this difference to lower osmotic pressure in 0.1 M solutions [40].

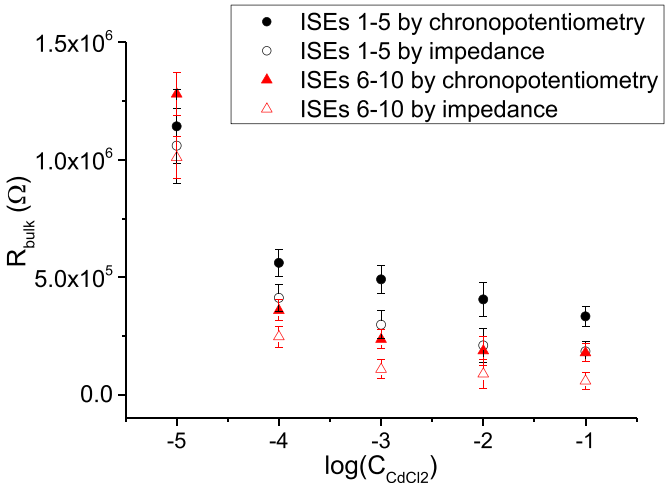

Fig. 7. The dependence of the membrane bulk resistances on the concentration of $CdCl_2$ in solution, measured by chronopotentiometry and by impedance.

However, it was shown that water uptake from deionized water is several times larger than that from 0.1 $CaCl_2$, and the authors assign this difference to lower osmotic pressure in 0.1 M solutions [40].

Our preliminary studies showed that when equilibrated with aqueous solutions of $CdCl_2$, membranes became turbid as shown in Fig. S6 (Supplementary Data) suggesting that absorbed water indeed forms droplets in the membranes. Also, the water uptake by Cd^{2+}-selective membranes was high (a few weight per-cents of the membrane itself), and can be registered by weighting dry membranes and membranes equilibrated with solutions. Therefore, we decided to undertake a systematic study of water uptake by our membranes.

Freshly prepared membranes, inevitably, contain some impurities of limited lipophilicity. Leak of these impurities may cause incorrect results. Therefore, the measurements were performed as follows. Initially, large pieces of membranes (ca 1 g) were weighted giving the mass value M_1. Next, the membrane pieces were placed into beakers with the respective solutions for 1 week, to be sure that the equilibrium is established (actually, the equilibration time was 2–3 days). Membranes equilibrated with solutions became turbid due to the Rayleigh scattering of light on the water droplets. After 1 week in solution, the membranes were pulled from the beakers and the membrane surfaces were gently dried with tissue paper, and after that weighted giving mass M_2: that of the membranes equilibrated with the respective solution. After that the membranes were dried in air until a constant mass M_3. Water fraction in the membranes was calculated as $M_W = (M_2 - M_3)/M_3$. Use of M_1 value instead of M_3 produced slightly biased results due to leak of low-lipophilic impurities. The bias was seen during the first 3 weeks of the studies. Apparently, 3 weeks of contact with solutions was enough for the low-lipophilic impurities to leak from the membranes.

The time needed for the complete evaporation of water from the membranes was 10–12 h. To be sure about the data we let the

membranes to dry for 24 h. An example of the membrane drying curve (the first 4.5 h) is shown in Fig. S7.

Water uptake was studied in two directions: first from 0.1 M $CdCl_2$ down to 10^{-5} M, to DI water, and then back to 0.1 M $CdCl_2$, and no hysteresis was registered. The results are presented in Fig. 8. One can see that the curves of the bulk resistance as a function of the solution concentration (Fig. 7) and that of the water uptake (Fig. 8) are very similar. In both cases the sensitivity to the concentration of $CdCl_2$ within the range from 0.1 to 0.001 M is low, and increases along further dilution. The similarity of the curves reveals a correlation between the membrane bulk resistance and water uptake, confirming our assumption about the role of water uptake in the non-constancy of the membrane bulk resistance.

3.5. SEM imaging of the membranes

Fast kinetics of the changes of the ISE bulk resistance, as shown in Fig. 4 and registered earlier also for Ca^{2+}- and K^{+}-ISEs suggests that the layers in the membrane which are responsible for these changes must be thin. According to some reports, water is not uniformly distributed within ISE membranes, and the layers in the vicinity of the membrane/solution interface are enriched in water [31,32,35,46]. This may be the reason for the fast kinetics of the changes of the membrane bulk resistance. SEM studies are performed under vacuum, and imaging of water by SEM/EDX technique is not possible. However, water droplets must contain the electrolyte from the bulk solution, and layers enriched in water (in wet membranes) could remain enriched in cadmium (in dry membranes). It was therefore interesting to measure the element profiles across the membranes in the vicinity of the surface by SEM/EDX technique. The membranes were equilibrated with 0.01 M $CdCl_2$, sliced in the direction perpendicular to the surface, and then SEM images were taken. Results obtained with membrane M1 without ETH 500 are shown in Fig. 9. Cavities in the membrane bulk, seen in the image, result from incomplete de-aeration of the cocktails during the manufacturing of the membranes. The results of EDX scanning show that the surface layers of the membrane (about 7–8 μm) are enriched in plasticizer and depleted in PVC: compare carbon, oxygen and chlorine profiles. This result is consistent with literature data [46]. The lipophilic ionophore contains sulfur in its structure. Therefore, the similarity of the cadmium and the sulfur profiles suggest that cadmium is predominantly in the organic phase. Profiles of cadmium and sulfur are noisy, two apparent "peaks" at about 10 and 35 μm deep hardly can be treated as a systematic effect. Studies of deeper layers also showed similar and roughly uniform distribution of cadmium and sulfur, see Fig. S7. The SEM/EDX studies of membrane M2 with ETH 500 delivered analogous results.

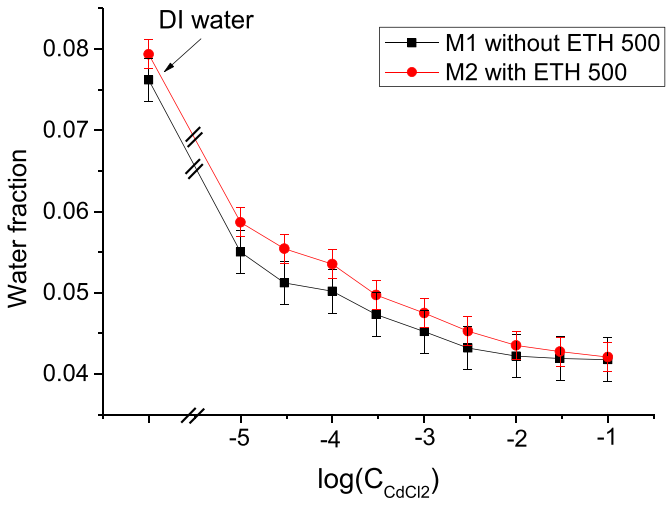

Fig. 8. Water uptake by the membranes.

4. Conclusions

The results obtained here with Cd^{2+}-ISE membranes are consistent with those obtained in our earlier studies with ISEs selective to calcium [25], nitrate [26] and potassium [27]. The membrane bulk resistance measured by means of chronopotentiometry and electrochemical impedance is not constant over the Nernstian potentiometric response range, which appears in conflict with the current views on the mechanism of the ISE response and, in particular, on the role of ion-exchange process at the membrane/solution interface. We already attributed this paradox to the consequences of the water uptake by the plasticized PVC membranes. In this work we specifically addressed the water uptake and its dependence on the concentration of the solution. The results revealed a similarity between the shapes of the curves depicting the resistance and the water content in the membranes vs. the concentration of the solution.

The role of the water uptake in the non-constancy of the membrane bulk resistance may be as follows. The presence of a dispersed aqueous phase in plasticized PVC membranes means that the real membranes when in contact with solutions are non-homogeneous: they consist of an organic phase proper and of water droplets. Apparently, the interfacial electrochemical equilibrium which is responsible for the potentiometric behavior of ISEs is established between the aqueous phase and the organic phase proper, whereas the resistance is a property of the membrane as a material.

Concerning the liquid in the droplets, at equilibrium its composition must be similar to that of the bulk solution. The respective electrolyte is confined to droplets and hardly contributes to charge transfer across the membranes. On the contrary, ionophores and ion-exchangers, as well as ion-ionophore complexes which counter-balance the charge of ion-exchanger sites are confined to the organic phase. The concentration of the potential-determining ions (in the form as ion-ionophore complexes) in the organic phase of the membranes is constant and equivalent to that of the ion-exchanger sites, and the ISEs show Nernstian or near-Nernstian potentiometric response. However, water droplets may act as barriers for the diffusion of lipophilic species, and in this way increase of the water uptake may results in increase of the membrane bulk resistance.

Furthermore, electric double layers around water droplets effectively form a network of capacitors which are simultaneously in parallel and in series with each other. Re-charging of this distributed capacitor consumes a large electric charge. This may explain the regularities of the polarization and relaxation in the chronopotentiometric measurements, and enormously high values of the respective capacitances.

Fig. S1: the electrode construct; Figs. S2 and S3: response curves obtained with ISEs; Figs. S4 and S5: examples of fitting of the polarization and relaxation curves; Fig. S6: photos of membrane M1 dry and equilibrated with deionized water; Fig. S7: kinetics of the evaporation of water from membranes; Fig. S8: element profiles across membrane M1; Table S1: the membrane bulk resistance obtained from the Ohmic drops in chronopotentiometric measurements.

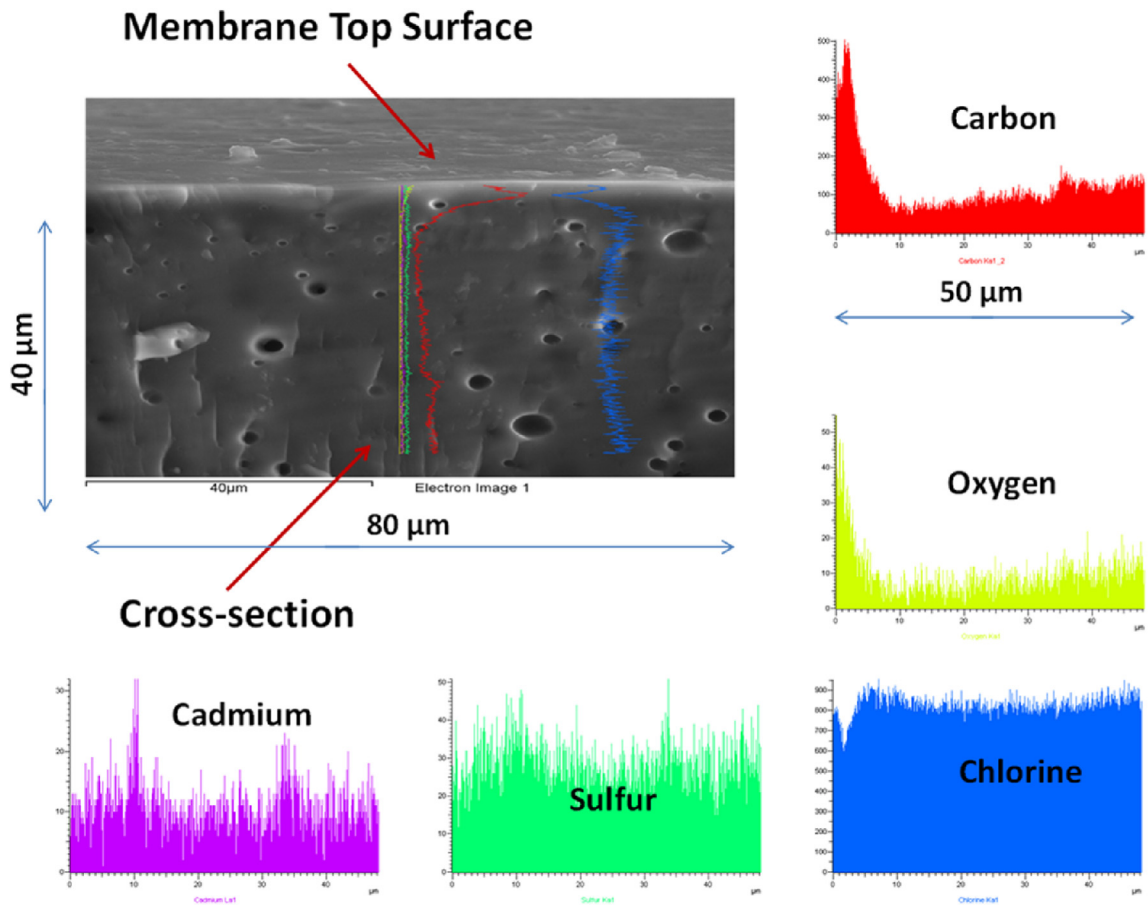

Fig. 9. SEM image of membrane M1 (top and cross-section), and element profiles over 50 µm from the membrane surface (EDX).

Acknowledgements

The authors acknowledge the Interdisciplinary Center for Nanotechnology of the Research Park of St. Petersburg State University for SEM/EDX imaging of the membranes. The study was performed with financial support from Russian Foundation for Basic Research, grant 19-03-00259.

Appendix A. Supplementary data

Supplementary data to this article can be found online at https://doi.org/10.1016/j.electacta.2019.135541.

References

[1] E. Zdrachek, E. Bakker, Potentiometric sensing, Anal. Chem. 91 (2019) 2, https://doi.org/10.1021/acs.analchem.8b04681.
[2] E. Bakker, P. Bühlmann, E. Pretsch, Carrier-based ion-selective electrodes and bulk optodes. 1. General characteristics, Chem. Rev. 97 (1997) 3083, https://doi.org/10.1021/cr940394a.
[3] P. Bühlmann, E. Pretsch, E. Bakker, Carrier-based ion-selective electrodes and bulk optodes. 2. Ionophores for potentiometric and optical sensors, Chem. Rev. 98 (1998) 1593, https://doi.org/10.1021/cr970113+.
[4] J. Bobacka, A. Ivaska, A. Lewenstam, Potentiometric ion sensors, Chem. Rev. 108 (2008) 329, https://doi.org/10.1021/cr068100w.
[5] K.N. Mikhelson, M.A. Peshkova, Advances and trends in ionophore-based chemical sensors, Russ. Chem. Rev. 84 (2015) 555, https://doi.org/10.1070/RCR4506.
[6] M.B. Garada, B. Kabagambe, A. Izadyar, S. Amemiya, Stripping voltammetry of nanomolar potassium and ammonium ions using a valinomycin-doped double-polymer electrode, Anal. Chem. 84 (2012) 7979, https://doi.org/10.1021/ac301773w.
[7] G.A. Crespo, M. Cuartero, E. Bakker, Thin layer ionophore-based membrane for multianalyte ion activity detection, Anal. Chem. 87 (2015) 7729, https://doi.org/10.1021/acs.analchem.5b01459.
[8] M. Cuartero, G.A. Crespo, E. Bakker, Ionophore-based voltammetric ion activity sensing with thin layer membranes, Anal. Chem. 88 (2016) 1654, https://doi.org/10.1021/acs.analchem.5b03611.
[9] P.J. Greenawalt, S. Amemiya, Voltammetric mechanism of multiion detection with thin ionophore-based polymeric membrane, Anal. Chem. 88 (2016) 5827, https://doi.org/10.1021/acs.analchem.6b00397.
[10] D. Yuan, M. Cuartero, G.A. Crespo, E. Bakker, Voltammetric thin-layer ionophore-based films: Part 1. Experimental evidence and numerical simulations, Anal. Chem. 89 (2017) 586, https://doi.org/10.1021/acs.analchem.9b0212689.
[11] D. Yuan, M. Cuartero M, G.A. Crespo, E. Bakker, Voltammetric thin-layer ionophore-based films: Part 2. Semi-empirical treatment, Anal. Chem. 89 (2017) 595, https://doi.org/10.1021/acs.analchem.6b03355.
[12] D. Kałuża, A. Michalska, K. Maksymiuk, Voltammetric Properties of All-solid State Ion-selective Electrodes with Multiwalled Carbon Nanotubes-poly(3-octylthiophene-2,5-diyl) Nanocomposite Transducer, Electroanalysis, 2019, https://doi.org/10.1002/elan.201900380.
[13] E. Hupa, U. Vanamo, J. Bobacka, Novel ion-to-electron transduction principle for solid-contact ISEs, Electroanalysis 27 (2015) 591, https://doi.org/10.1002/elan.201400596.
[14] U. Vanamo, E. Hupa, V. Yrjänä, J. Bobacka, New signal readout principle for solid-contact ion-selective electrodes, Anal. Chem. 88 (2016) 4369, https://doi.org/10.1021/acs.analchem.5b04800.
[15] T. Han, U. Vanamo, J. Bobacka, Influence of electrode geometry on the response of solid-contact ion-selective electrodes when utilizing a new coulometric signal readout method, ChemElectroChem 3 (2016) 2071, https://doi.org/10.1002/celc.201600575.
[16] Z. Jarolímová, T. Han, U. Mattinen, J. Bobacka, E. Bakker, Capacitive model for coulometric readout of ion-selective electrodes, Anal. Chem. 90 (2018) 8700, https://doi.org/10.1021/acs.analchem.8b02145.
[17] T. Han, U. Mattinen, J. Bobacka, Improving the sensitivity of solid-contact ion-selective electrodes by using coulometric signal transduction, ACS Sens. 4 (2019) 900, https://doi.org/10.1021/acssensors.8b01649.
[18] E. Jaworska, P. Pawłowski, A. Michalska, K. Maksymiuk, Advantages of amperometric readout mode of ion-selective electrodes under potentiostatic conditions, Electroanalysis 31 (2019) 343, https://doi.org/10.1002/elan.201800649.

[19] W.E. Morf, The Principles of Ion-Selective Electrodes and of Membrane Transport, Akademiai Kiado, Budapest, 1981.
[20] K.N. Mikhelson, Ion-selective Electrodes (Lecture Notes in Chemistry, vol. 81, Springer, Heidelberg-New York-Dordrecht-London, 2013, https://doi.org/10.1007/978-3-642-36886-8.
[21] T. Sokalski, A. Lewenstam, Application of Nernst-Planck and Poisson equations for interpretation of liquid-junction and membrane potentials in real-time and space domains, Electrochem. Commun. 3 (2001) 107, https://doi.org/10.1016/S1388-2481(01)00110.
[22] J.J. Jasielec, T. Sokalski, R. Filipek, A. Lewenstam, Comparison of different approaches to the description of the detection limit of ion-selective electrodes, Electrochim. Acta 55 (2010) 6836, https://doi.org/10.1016/j.electacta.2010.05.083.
[23] K. Szyszkiewicz, M. Danielewski, J. Fausek, J.J. Jasielec, W. Kucza, A. Lewenstam, T. Sokalski, R. Filipek, Breakthrough in modeling of electro-diffusion processes : continuation and extensions of the classical work of Richard Buck, ECS Transactions 61 (2014) 21, https://doi.org/10.1149/06115.0021ecst.
[24] J.J. Jasielec, T. Sokalska, R. Filipek, A. Lewenstam, Neutral-Carrier ion-selective electrodes assessed by the Nernst−Planck−Poisson model, Anal. Chem. 87 (2015) 8665.
[25] YeO. Kondratyeva, E.V. Solovyeva, G.A. Khripoun, K.N. Mikhelson, Non-constancy of the bulk resistance of ionophore-based ion-selective electrode: a result of electrolyte co-extraction or of something else? Electrochim. Acta 259 (2018) 458, https://doi.org/10.1016/j.electacta.2017.10.176.
[26] A. Ivanova, K. Mikhelson, Electrochemical properties of nitrate-selective electrodes: the dependence of resistance on the solution concentration, MDPI Sensors 18 (2018) 2062, https://doi.org/10.3390/s18072062.
[27] Ye.O. Kondratyeva, E.V. Solovyeva, G.A. Khripoun, K.N. Mikhelson, Paradox of the variation of the bulk resistance of potassium ion-selective electrode membranes within nernstian potentiometric response range, Russ, J. Electrochemistry 55 (2019) 1118, https://doi.org/10.1134/S1023193519110090.
[28] E. Bakker, P. Bühlmann, E. Pretsch, The phase-boundary potential model, Talanta 63 (2004) 3, https://doi.org/10.1016/j.talanta.2003.10.006.
[29] A.E. Shvarev, D.A. Rantsan, K.N. Mikhelson, Potassium-selective conductometric sensor, Sens. Actuators, B 76 (2001) 500.
[30] A.P. Thoma, A. Viviani-Nauer, S. Arvanitis, W.E. Morf, W. Simon, Mechanism of neutral carrier mediated ion transport through ion-selective bulk membranes, Anal. Chem. 49 (1977) 1567, https://doi.org/10.1021/ac50019a027.
[31] J.D. Harrison, X. Li, Measurement of concentration profiles inside a nitrite ion selective electrode membrane, Anal. Chem. 63 (1991) 2168, https://doi.org/10.1021/ac00019a018.
[32] A.D.C. Chan, X. Li, J.D. Harrison, Evidence for a water-rich surface region in poli(vinyl chloride)-based ion-selective electrode membranes, Anal. Chem. 64 (1992) 2512.
[33] A.D.C. Chan, J.D. Harrison, NMR study of the water in ion-selective electrode membrane, Anal. Chem. 65 (1993) 32.
[34] Z. Li, X. Li, S. Petrovic, D.J. Harrison, Dual-sorption model of water uptake in poly(vinyl chloride)-based ion-selective membranes: experimental water concentration and transport parameters, Anal. Chem. 68 (1996) 1717, https://doi.org/10.1021/ac950557a.
[35] T. Zwickl, B. Schneider, E. Lindner, T. Sokalski, U. Schaller, E. Pretsch, Chromoionophore-mediated imaging of water transport in ion-selective membranes, Anal. Sci. 14 (1998) 57, https://doi.org/10.2116/analsci.14.57.
[36] T. Lindfors, F. Sundfors, L. Höfler, R.E. Gyurcsányi, FTIR-ATR study of water uptake and diffusion through ion-selective membranes based on plasticized poly(vinyl chloride), Electroanalysis 21 (2009) 1914, https://doi.org/10.1002/elan.200904609.
[37] T. Lindfors, F. Sundfors, L. Höfler, R.E. Gyurcsányi, The water uptake of plasticized poly(vinyl chloride) solid-contact calcium-selective electrodes, Electroanalysis 23 (2011) 2156, https://doi.org/10.1002/elan.201100219.
[38] T. Lindfors, L. Höfler, G. Jágerszki, R.E. Gyurcsányi, Hyphenated FT-IR-attenuated total reflection and electrochemical impedance spectroscopy technique to study the water uptake and potential stability of polymeric solid-contact ion-selective electrodes, Anal. Chem. 83 (2011) 4902, https://doi.org/10.1021/ac200597b.
[39] F. Sundfors, T. Lindfors, L. Höfler, R. Bereczki, R.E. Gyurcsányi, FTIR-ATR study of water uptake and diffusion through ion-selective membranes based on poly(acrylates) and silicone rubber, Anal. Chem. 81 (2009) 5925, https://doi.org/10.1021/ac900727w.
[40] N. He, T. Lindfors, Determination of water uptake of polymeric ion-selective membranes with the coulometric Karl Fischer and FT-IR-attenuated total reflection techniques, Anal. Chem. 85 (2013) 1006, https://doi.org/10.1021/ac3027838.
[41] K.N. Mikhelson, J. Bobacka, A. Ivaska, A. Lewenstam, M. Bochenska, Selectivity of lithium electrodes: correlation with ion-ionophore complex stability constants and with interfacial exchange current densities, Anal. Chem. 74 (2002) 518, https://doi.org/10.1021/ac0155660.
[42] A.D. Ivanova, E.S. Koltashova, E.V. Solovyeva, M.A. Peshkova, K.N. Mikhelson, Impact of the electrolyte Co-extraction to the response of the ionophore-based ion-selective electrodes, Electrochim. Acta 214 (2016) 439, https://doi.org/10.1016/j.electacta.2016.07.142.
[43] J. Dvorak, J. Koryta, V. Bohackova, Elektrochemie, Academia, Praha, 1975.
[44] H.A. Arida, J.P. Kloock, M.J. Schöning, Novel organic membrane-based thin-film microsensors for the determination of heavy metal cations, MDPI Sensors 6 (2006) 435, https://doi.org/10.3390/s6040435.
[45] E. Bakker, R.K. Meruva, E. Pretsch, M.E. Meyerhoff, Selectivity of polymer membrane-based ion-selective electrodes: self-consistent model describing the potentiometric response in mixed ion solutions of different charge, Anal. Chem. 66 (1994) 3021, https://doi.org/10.1021/ac00091a600.
[46] Q. Ye, Z. Keresztes, G. Horvai, Characterization of the outmost surface of ion-selective solvent polymeric PVC membranes and protein adsorption, Electroanalysis 11 (1999) 729.